Advances in Colloid and Interface Science 183–184 (2012) 55–67

Contents lists available at SciVerse ScienceDirect

Advances in Colloid and Interface Science

journal homepage: www.elsevier.com/locate/cis

Determination of the aggregation number and charge of ionic surfactant micelles from the stepwise thinning of foam films

Svetoslav E. Anachkov [a], Krassimir D. Danov [a], Elka S. Basheva [a], Peter A. Kralchevsky [a,*], Kavssery P. Ananthapadmanabhan [b]

[a] Department of Chemical Engineering, Faculty of Chemistry and Pharmacy, Sofia University, Sofia 1164, Bulgaria
[b] Unilever Research & Development, 40 Merritt Blvd., Trumbull, CT 06611, USA

ARTICLE INFO

Available online 18 August 2012

Keywords:
Charge of surfactant micelles
Micelle aggregation number
Degree of micelle ionization
Stepwise thinning of foam films
Stratification

ABSTRACT

The stepwise thinning (stratification) of liquid films, which contain micelles of an ionic surfactant, depends on the micelle aggregation number, N_{agg}, and charge, Z. Vice versa, from the height of the step and the final film thickness one can determine N_{agg}, Z, and the degree of micelle ionization. The determination of N_{agg} is based on the experimental fact that the step height is equal to the inverse cubic root of the micelle concentration. In addition, Z is determined from the final thickness of the film, which depends on the concentration of counterions dissociated from the micelles in the bulk. The method is applied to micellar solutions of six surfactants, both anionic and cationic: sodium dodecylsulfate (SDS), cetyl trimethylammonium bromide (CTAB), cetylpyridinium chloride (CPC), sodium laurylethersulfates with 1 and 3 ethylene oxide groups (SLES-1EO and SLES-3EO), and potassium myristate. The method has the following advantages: (i) N_{agg} and Z are determined simultaneously, from the same set of experimental data; (ii) N_{agg} and Z are determined for each given surfactant concentration (i.e. their concentration dependence is obtained), and (iii) N_{agg} and Z can be determined even for turbid solutions, like those of carboxylates, where the micelles coexist with acid-soap crystallites, so that the application of other methods is difficult. The results indicate that the micelles of greater aggregation number have a lower degree of ionization, which can be explained with the effect of counterion binding. The proposed method is applicable to the concentration range, in which the films stratify and the micelles are spherical. This is satisfied for numerous systems representing scientific and practical interest.

Contents

* Corresponding author.
E-mail address: pk@lcpe.uni-sofia.bg (P.A. Kralchevsky).

0001-8686/$ – see front matter © 2012 Elsevier B.V. All rights reserved.
http://dx.doi.org/10.1016/j.cis.2012.08.003

1. Introduction

The stepwise thinning (stratification) of foam and emulsion films containing surfactant micelles or spherical nanoparticles represents a layer-by-layer thinning of an ordered particle structure inside the film [1–5] and can be considered as a manifestation of the oscillatory structural surface forces [6–10]. Knowing the particle size, concentration and interactions, it is possible to predict the behavior of such films by means of theoretical models [11–14] and computer simulations [15–20]. Detailed reviews on thin film stratification were given in recent articles [21–23].

Here we focus on the inverse problem, viz. to obtain information for the surfactant micelles from the stepwise thinning of liquid films. In the case of *nonionic* micelles, the interpretation of the stratification data with an appropriate hard-sphere model yields the micelle aggregation number, N_{agg} [21,24]. In the case of *ionic* surfactants, the situation is more complicated because the electrostatic force between the charged micelles is soft and long-range [25,26], and the height of the stratification steps, Δh, is considerably greater than the micelle hydrodynamic diameter [23]. Fortunately, the experiment and computer simulations provide a simple relation between Δh and the micelle (particle) concentration [1,2,18,27–29], which can be directly used for determining N_{agg} [23]; see Section 3 in the present article. Extending the analysis in Ref. [23], here we demonstrate that the degree of micelle ionization, α, can be determined from the final film thickness, h_0, which is established at the end of the stepwise thinning of the liquid film. In this final state, the film contains (almost) no micelles, but its thickness is influenced by the counterions dissociated from the micelles in the bulk, which increase the Debye screening of the electrostatic repulsion and the osmotic pressure of the bulk phase. Knowing the theoretical relationship between α and h_0, one can determine α from the experimentally measured h_0 (Section 4). In this way, the micelle charge, $Z = \alpha N_{agg}$, is also determined.

The most widely used method for determining the micelle ionization degree, α, is by electrolytic conductivity, from the slope of the conductivity plot above the critical micellization concentration (CMC) [30–36]. Theoretical models for determining not only α but also N_{agg} from the conductivity data have been proposed [37–40]. α can be determined also from the mass action law applied to the dependence of CMC on the counterion concentration [41,42]; by measuring electromotive force (by ion selective electrodes) [43–48]; by equilibrium dialysis [49]; from the osmotic coefficient [50] and Krafft temperature [51]; by electrophoresis and zeta-potential measurements [52–54], by chemical trapping of free counterions [55] and electron paramagnetic resonance (EPR) spectroscopy [56]. In addition, the micelle aggregation number, N_{agg}, can be determined by light scattering [57]; fluorescence quenching [58–62] and time-resolved fluorescence quenching [63–66]; EPR [66,67]; nuclear magnetic resonance (NMR) spectroscopy [68,69]; small-angle X-ray scattering (SAXS) [70], and small-angle neutron scattering (SANS) [66].

Depending on the used experimental method and model for data interpretation, rather different values of α have been reported in the literature for the same system. For example, for micelles of sodium dodecylsulfate (SDS) $\alpha = 0.14$ was obtained by electromotive-force measurements of the activity of Na^+ ions [44], whereas $\alpha = 0.54$ was determined from the dependence of CMC on the Na^+ concentration [41,42]. Low values, $\alpha = 0.05$ for SDS micelles, and 0.08 for cetylpyridinium chloride (CPC) micelles, were obtained by theoretical analysis of data for the solutions' osmotic pressure [71]. In other words, the problem is how to determine the true value of α.

Additional difficulty is related to the fact that both Z and N_{agg} (and their ratio α) depend on the concentration of the ionic surfactant and added salt; see e.g. [72]. In other words, the values of Z, N_{agg} and α have to be determined at each given surfactant and salt concentrations. From this viewpoint, methods for determining α from the slope of experimental plots of data for conductivity vs. surfactant concentration [23] or of the critical micellization concentration (CMC) vs. counterion concentration [41,42] can give only a mean (effective) value of α.

The method proposed here allows determination of both N_{agg} and α at each given surfactant concentration from the experimental dependence of the film thickness, h, on time, t, for stratifying films from ionic surfactant solutions. The theoretical interpretation of the experimental data is physically transparent and has been already tested in our previous study [23]. The proposed method is quite different from the aforementioned methods and may help in establishing reliable values of N_{agg}, Z and α for the micelles of ionic surfactants.

2. Experimental section

2.1. Materials

In our experiments, foam films were formed from micellar solutions of three surfactants. The first two of them are sodium laurylethersulfates with 1 and 3 ethylene oxide groups denoted, respectively, SLES-1EO and SLES-3EO. They are products of Stepan Co. with commercial names STEOL CS-170 and STEOL CS-330, and molecular masses 332.4 and 420.5 g/mol. Their critical micellization concentrations (CMC) measured by both surface tension and electrolytic conductivity are, respectively, 0.7 and 0.5 mM at 25 °C [73,74].

The third surfactant is potassium tetradecanoate (myristate), denoted KMy, product of Viva Co., of molecular mass 266.46 g/mol and CMC = 10 mM at 25 °C [75]. The experiments were carried out at the solution's natural pH, at which the KMy micelles coexist with crystallites of 1:1 acid soap [75]. Because the crystallites are much larger than the micelles, they dominate the light scattering from the KMy solutions, so that determination of the micelle size and aggregation number by light-scattering is impossible. In thinning liquid films, the crystallites are carried away by the hydrodynamic flow, whereas the KMy micelles give rise to a stepwise thinning of the films (see below).

Here, we analyze also data from our previous paper [23] for three other surfactants: sodium dodecyl sulfate (SDS, anionic; molecular mass 288.38 g/mol; product of Across Organics); cetyl trimethylammonium bromide (CTAB, cationic; molecular mass 364.45 g/mol; product of Sigma) and cetylpyridinium chloride (CPC, cationic; molecular mass 339.99 g/mol; product of Sigma).

All experiments have been performed at a temperature of 25 °C. Inorganic salts (e.g. NaCl) have not been added, because they suppress the film stratification (at sufficiently high concentrations).

2.2. Experimental method

The film thickness, h, vs. time, t, was measured by means of the Scheludko–Exerowa (SE) cell [76,77] in reflected monochromatic

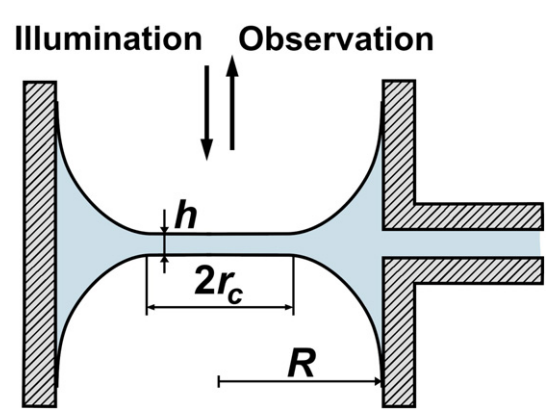

Fig. 1. The SE cell [76,77] represents a cylindrical glass capillary (of inner radius R = 1.5 mm), which is filled with the working solution. A portion of the liquid is sucked out from the cell through the orifice in the wall. In the central part of the cell, a liquid film of radius r_c is formed, which is encircled by a Plateau border; h is the film thickness.

light of wavelength 546 nm; see Fig. 1. The investigated solution is loaded in a cylindrical capillary through an orifice in its wall. Thus, a biconcave drop is formed inside the capillary. Next, liquid is sucked through the orifice and the two menisci approach each other until a liquid film is formed in the central part of the cell. By injecting or sucking liquid through the orifice, one can vary the radius of the formed film. Its thickness can be measured by means of an interferometric method [2,77,78]. For this purpose, the light reflected from the film is registered by a photomultiplier and computer, and the film thickness is recorded in the course of the experiment. The SE cell is placed in a closed container, so that the water vapor is equilibrated with the solution, and evaporation from the film is prevented. Details on the used experimental method can be found in Ref. [2,21].

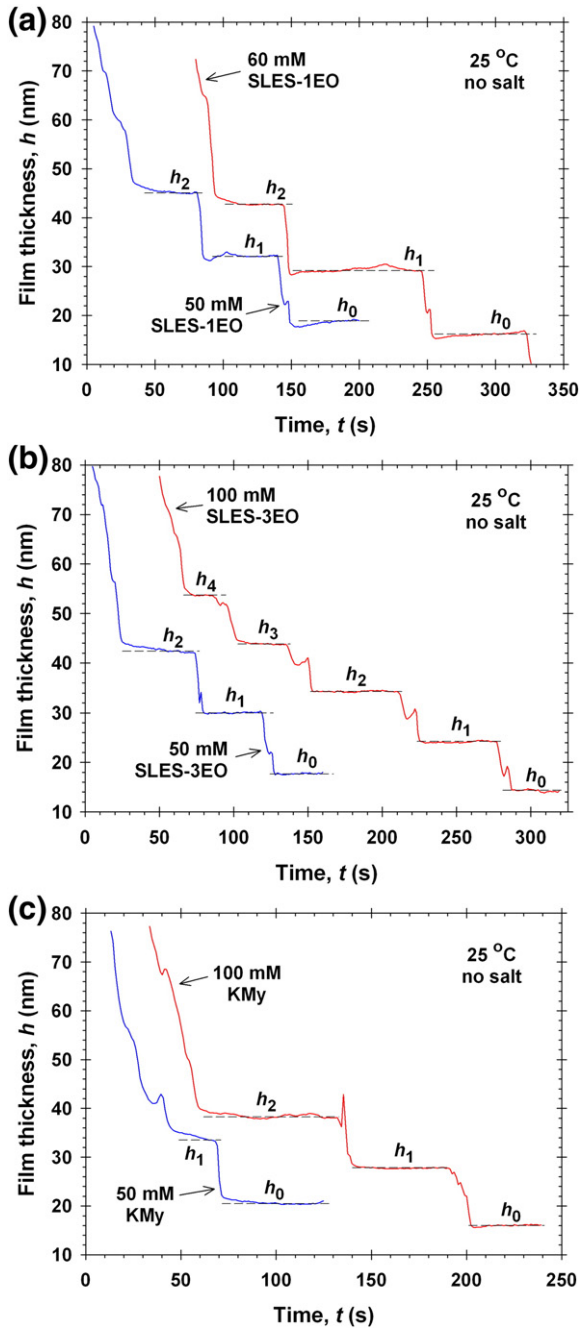

Fig. 2. Experimental time dependence, $h(t)$, of the equivalent water thickness of foam films in a SE cell: (a) 50 mM and 60 mM SLES-1EO; (b) 50 mM and 100 mM SLES-3EO; (c) 50 mM and 100 mM KMy; h_k, is the thicknesses of the metastable state with k micellar layers inside the film; $k = 0, 1, 2, \ldots$.

The foam films from the investigated micellar solutions exhibit stepwise thinning; see Fig. 2. Experimentally, it is realized by the appearance and expansion of darker spots (of smaller thickness) in the film [4]. The microscope diaphragm is almost closed, so that the light reflected from a small part of the film is supplied to the photomultiplier. The passing of the border of an expanding spot through the observation field is registered as a step (Fig. 2). Each step corresponds to a metastable state of the film that contains a given number of micellar layers inside the film [1–5], as illustrated in Fig. 3. The thicknesses of the films that contain 1, 2, 3, … layers of micelles are denoted by h_1, h_2, h_3, etc. The thickness of the final state of the film will be denoted by h_0. In this state, the film does not contain micellar layers, but it may contain isolated micelles if its thickness is greater than the micelle diameter [23].

The inner radius of the used SE cell was $R = 1.5$ mm (Fig. 1). The typical radius of the formed foam films is $r_c \approx 0.1$ mm. Under such conditions, the sucking capillary pressure applied to the SE cell can be estimated as $P_c \approx 2\sigma/R$, where σ is the solution's surface tension. Table 1 summarizes the experimental values of CMC; the values of σ at CMC (which are almost constant in the experimental concentration range ≥ CMC); the estimated values of P_c and the summary thickness of the two surfactant adsorption layers, h_a, for the 6 investigated surfactants. The value of h_a equals the doubled length of the extended surfactant molecule, including the diameter of the hydrated counterion (Fig. 3), and is obtained by molecular-size considerations, in the same way, in which the micelle diameter was estimated in Ref. [23]. The data in Table 1 will be used to analyze theoretically the obtained experimental results.

2.3. Experimental results

Fig. 2 shows typical experimental curves for the step-wise thinning of foam films formed from micellar solutions of SLES-1EO, SLES-3EO and KMy. At higher surfactant concentrations, more stepwise transitions are observed. The data indicate that the height of the steps, Δh, is practically the same at a given surfactant concentration, i.e. $h_1 - h_0 = h_2 - h_1 = h_3 - h_2 = \ldots = \Delta h$. In general, Δh decreases with the rise of the total input surfactant concentration, c_s. As mentioned above, in the case of KMy, the solutions contain crystallites of acid soap, coexisting with the micelles [75]. During the film thinning, the crystallites were driven away by the hydrodynamic flow and after that one or two stepwise transitions in the film thickness were observed.

The data for the experimental step height Δh and final film thickness h_0, measured at different surfactant concentrations c_s, are

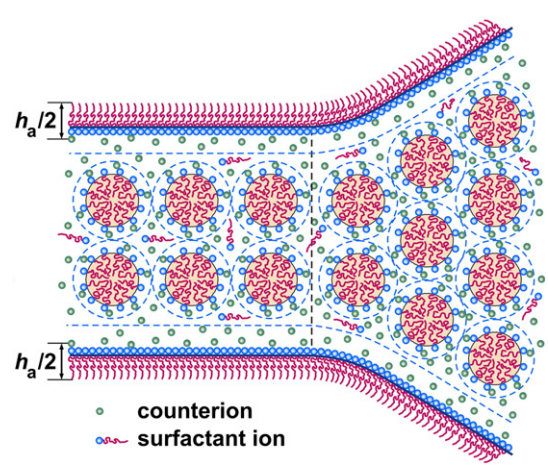

Fig. 3. Osmotic equilibrium between the film and Plateau border: because the osmotic pressure of the micelles (dominated by the dissociated counterions) is much greater than the capillary pressure, the concentrations of micelles in the film and Plateau border must be (approximately) equal.

Table 1
Values of CMC, of the respective surface tension, σ_{CMC}; of the capillary pressure P_c, and total thickness of the two adsorption layers at the film surfaces, h_a.

Surfactant	CMC (mM)	σ_{CMC} (mN/m)	P_c (Pa)	h_a (nm)
SDS	8	39	52	5.26
CTAB	0.9	37	49	6.40
CPC	0.9	42	56	6.50
SLES-1EO	0.7	33	44	5.64
SLES-3EO	0.5	33	44	6.40
KMy	10	33	44	5.21

summarized in Table 2. Each value in this table is the average for at least 25 experiments with separate foam films.

In general, Δh is considerably greater than the hydrodynamic diameter of the micelle, d_H, which is practically equal to h_a (Fig. 3) — compare the values of h_a and Δh in Tables 1 and 2. For example, at 50 mM KMy, $\Delta h = 15$ nm (Table 2), whereas $d_H \approx h_a \approx 5.2$ nm (Table 1). The difference between Δh and d_H is due to the electrostatic repulsion between the micelles, which results in a greater effective size of the micelles [2,23].

The final film thickness, h_0, is also greater than $d_H \approx h_a$: compare Tables 1 and 2. Hence, in principle it is possible for isolated micelles to penetrate in the final film of thickness h_0. From the values of Δh and h_0 in Table 2, we determine the micelle aggregation number, N_{agg}, and charge, Z, as explained in Sections 3 and 4.

Table 2
Experimental step height Δh and final film thickness h_0 vs. the surfactant concentration c_s.

Concentration, c_s (mM)	Step height, Δh (nm)	Final thickness, h_0 (nm)
SDS[a]		
30	15.3	22.2
40	14.7	18.6
50	13.7	17.3
100	10.6	13.5
CTAB[a]		
10	25.8	46.8
20	21.8	34.3
30	19.9	28.2
40	18.0	25.2
50	16.6	22.3
CPC[a]		
10	21.2	41.7
20	18.7	30.6
30	16.6	25.7
40	15.8	22.7
50	14.6	20.8
SLES-1EO		
40	14.2	20.5
50	13.4	18.3
60	13.0	16.4
SLES-3EO		
30	13.7	20.0
40	12.6	19.1
50	12.2	17.6
100	10.0	13.8
KMy		
50	15.0	20.0
100	11.6	14.2

[a] Data from Ref. [23].

3. Determination of N_{agg} from the experimental value of Δh

3.1. The inverse-cubic-root law: experiments and computer modeling

First, Nikolov et al. [1,2] established experimentally that the measured values of Δh for micellar solutions of the anionic surfactant SDS are practically equal to the average distance, $\delta_I \equiv c_p^{-1/3}$, between two micelles in the bulk of solution, viz.

$$\Delta h \approx \delta_I \equiv c_p^{-1/3} = \left(\frac{c_s - \mathrm{CMC}}{N_{agg}}\right)^{-1/3}. \quad (1)$$

Here, c_p is the number of micelles (charged particles) per unit volume of the solution (suspension); c_s and CMC are the total input surfactant concentration and the critical micellization concentration expressed as number of molecules per unit volume; as usual, N_{agg} is the mean micelle aggregation number.

Subsequently, the inverse-cubic-root law, $\Delta h \propto c_p^{-1/3}$, was obtained by Jönsson et al. [79] by Monte Carlo (MC) simulations and density-functional-theory (DFT) calculations for charged macromolecules (spherical macroions) confined between two plane-parallel walls. In this case, Δh refers to the period of the calculated disjoining pressure. In the case of polyelectrolytes, the $\Delta h \propto c_p^{-1/3}$ law refers to coil (quasi-spherical) conformations. In the case of extended polyelectrolyte chains, another law, $\Delta h \propto c_p^{-1/2}$, has been experimentally established [80–82].

By using colloidal probe atomic force microscope (CP-AFM), Piech and Walz [27] found out that the period of the measured oscillatory force across a film from suspension of 22 nm sized charged silica particles obeys the $\Delta h = c_p^{-1/3}$ empirical law. In the case of polyelectrolyte coils, these authors found $\Delta h \propto c_p^{-1/3}$ in the dilute regime, and $\Delta h \propto c_p^{-1/2}$ in the semi-dilute regime (overlapping polymer chains). The dependence $\Delta h = c_p^{-1/3}$ was confirmed in subsequent experiments with both charged silica spheres and SDS micelles by Walz et al. [28]. More precisely $\Delta h = a c_p^{-1/3}$ with $a = 0.86$ was obtained using a specific set of experimental data for the N_{agg} of SDS obtained by a fluorescence quenching method [72].

Note that in the case of micelles, c_p is not an input parameter (as for particles) but it is calculated from c_s at a given N_{agg}; see Eq. (1). In general, N_{agg} is not constant — it increases with the concentration of ionic surfactant. In all cases, N_{agg} is calculated from experimental data using a theoretical model related to the specific experimental method. Depending on the used method and model, the obtained values of N_{agg} for the same system vary in a certain range (see below). So, if c_p is calculated from Eq. (1) for micellar solutions using data for N_{agg} from different sources, the difference between the curves with $a = 0.86$ and $a = 1$ in Fig. 5 of Ref. [28] would fall into the range of scattering of the calculated c_p. The law $\Delta h = c_p^{-1/3}$ should be valid not only for charged solid particles, but also for ionic surfactant micelles (as far as they are also charged particles), if the correct values of N_{agg} are used to calculate c_p from Eq. (1).

In a series of papers, Klapp et al. [16–20,29,83] investigated theoretically and experimentally the oscillatory surface forces due to the confinement of suspensions of charged nanoparticles between two solid surfaces in relation to the characteristic distance between the particles in the bulk. In Ref. [17], the bulk suspension was described theoretically by using the integral equations of statistical mechanics in the frame of the hypernetted chain (HNC) approximation, whereas the bulk structure factor was experimentally determined by small angle neutron scattering (SANS). In addition, the surface force of the film was calculated by MC simulations and measured by CP-AFM. In both cases (bulk suspension and thin film) excellent agreement between theory and experiment was established and the obtained data for the characteristic spatial period obey the $\Delta h \propto c_p^{-1/3}$ law. At higher ionic strengths, deviations from the above law were observed

[17]. Agreement between theory and experiment was obtained also in Ref. [16,18], where the results from the DFT and MC calculations were compared with CP-AFM and SANS results, and it was established that the $\Delta h \propto c_p^{-1/3}$ law is fulfilled for ionic strengths $I<10^{-3}$ M due to added salt. At $I \geq 10^{-3}$ M, the force oscillations were found to essentially disappear [18].

If the experimental and calculated data are plotted vs. the particle volume fraction, ϕ, then different Δh vs. ϕ curves are obtained for different values of the particle radius R [83]. Note that $c_p^{-1/3} = (4\pi/3)^{1/3} R\phi^{-1/3} \approx 1.612\ R\phi^{-1/3}$. In Ref. [29], it was demonstrated that the data obtained at various R collapse onto a single master curve, $\Delta h = c_p^{-1/3}$, if they are plotted vs. c_p, rather than vs. ϕ. This is illustrated in Fig. 4, where data from Ref. [29] for three different particle diameters, 11, 16 and 26 nm, are plotted. The data for the period of the bulk structure factor, measured by small angle X-ray scattering (SAXS), and for the period of the oscillatory surface force in a film, measured with CP-AFM, are complying with the same $\Delta h = c_p^{-1/3}$ dependence (Fig. 4). This once again confirms the coincidence of the film step height Δh with the mean distance between the charged particles (micelles) in the bulk.

In summary, the validity of the $\Delta h = c_p^{-1/3}$ law has been experimentally established in a series of studies by different methods: with thin foam films using the SE cell [1,2]; by CP-AFM measurements supported by SANS and SAXS experiments [16–19,27–29,83]. In addition, the $\Delta h = c_p^{-1/3}$ dependence has been theoretically predicted by the density functional calculations and MC simulations [16–20,29,79,83]. This law is satisfied in a wide range of particle concentrations (Fig. 4). Its validity is limited at low and high particle concentrations, characterized by the effective particle volume fraction (particle + counterion atmosphere) [29]. The decrease of the effective particle volume fraction can be experimentally accomplished not only by dilution, but also by addition of electrolyte that leads to shrinking of the counterion atmosphere.

In the other limit, the violation of the $\Delta h = c_p^{-1/3}$ law at higher charged-particle concentrations is related to the appearance of a freezing transition in suspensions sandwiched between two walls, that has been established by MC simulations [20]. Such a deviation at high concentrations was experimentally detected in CP-AFM experiments with silica-particle suspensions [28]. After the addition of some amount of electrolyte (KNO_3), the data for the same concentrated suspensions again comply with the $\Delta h = c_p^{-1/3}$ law. This can be explained with the fact that the added electrolyte has shrunk the counterion atmospheres and decreased the effective volume fraction of the charged particles below the freezing transition threshold [20].

In conclusion, the $\Delta h = c_p^{-1/3}$ law is fulfilled in a wide range of particle concentrations (Fig. 4) that coincides with the range where stratification (step-wise thinning) of free liquid films formed from particle suspension

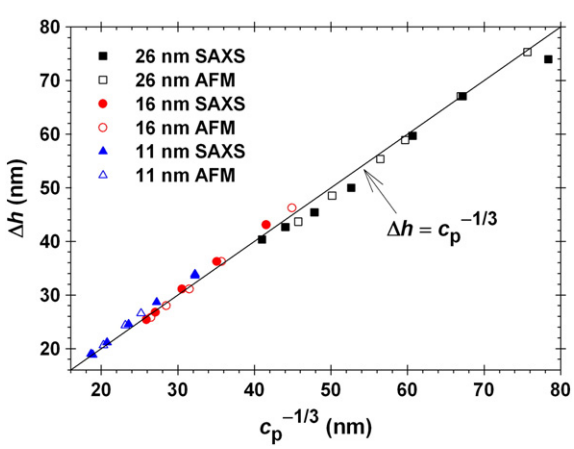

Fig. 4. Illustration of the inverse-cubic-root law, $\Delta h = c_p^{-1/3}$, with experimental data from Fig. 4 in Ref. [29] for suspensions from charged silica particles of diameters 11, 16 and 26 nm. The full symbols are data for the spatial period of the bulk structure factor measured by SAXS; the empty symbols are data for the period of the structural surface force measured by CP-AFM.

and micellar solution is observed [23]. Consequently, Eq. (1) can be used to determine the aggregation number of the micelles of an ionic surfactant, N_{agg}, from the measured stratification height steps, Δh [23]:

$$N_{agg} = (c_s - \mathrm{CMC})(\Delta h)^3. \tag{2}$$

In Eq. (2), c_s and CMC have to be expressed as number of molecules per unit volume. Comparison of the values of N_{agg} determined from Eq. (2) with the values obtained by other methods is given in Section 3.3.

3.2. Interpretation of the inverse-cubic-root law

The fact that $a = 1$ in the law $\Delta h = a c_p^{-1/3}$ was established by both experimental measurements and computer modeling [18,23,28,29]; see e.g. Fig. 4. Hence, one can conclude that in the concentration range where this law is fulfilled, the particles near a wall, or between two walls, are located in layers parallel to the wall and separated at an average layer-to-layer distance equal to $c_p^{-1/3}$. Inside such a layer, the particles have no lateral ordering. Indeed, as established by MC simulations [20], the lateral ordering appears at relatively high particle volume fractions, e.g. $\phi \geq 0.56$, which is at the upper limit of validity of the $\Delta h = c_p^{-1/3}$ law.

An interpretation of the $\Delta h = c_p^{-1/3}$ relation as an osmotic-pressure balance between the film and the bulk was given in Ref. [23]. Because of the large number of dissociated counterions, the micelles (the charged particles) give a considerable contribution to the osmotic pressure. The disjoining pressure is approximately equal to the difference between the osmotic pressures in the film and in the bulk: $\Pi \approx P_{osm}(h) - P_{osm}(\infty)$. (In first approximation, the van der Waals component of Π can be neglected for equilibrium films containing charged particles or micelles.) Under typical experimental conditions, Π is a small difference between two much greater quantities, i.e. $P_{osm}(h) \approx P_{osm}(\infty)$. In other words, the osmotic pressures of the micelles in the film and in the bulk are approximately equal, and consequently, the respective average micelle concentrations in the film and in the bulk have to be practically the same (Fig. 3). Note that this osmotic-pressure interpretation essentially uses the presence of macroions with numerous dissociated counterions. This situation is rather different from the case of non-charged molecules considered by Raman [84], who obtained $\Delta h = 0.554\ c_p^{-1/3}$ for the average distance between two molecules in an ideal gas of number density c_p.

Experimentally, Δh is considerably greater than the diameter of the particle (micelle), itself; see e.g. Section 2.3 and Fig. 4. Δh can be considered as an effective diameter of the charged particle, d_{eff}, which includes its counterion atmosphere. A semiempirical expression for calculating Δh was proposed in Ref. [23]:

$$d_{eff} = 2R\left\{1 + \frac{3}{(2R)^3}\int_{2R}^{\infty}\left[1 - \exp\left(-\frac{3u_{el}(r)}{kT}\right)\right] r^2 dr\right\}^{1/3} \tag{3}$$

where R is the radius of the particle (micelle) itself (without the counterion atmosphere); k is the Boltzmann constant; T is the absolute temperature, and $u_{el}(r)$ is the energy of electrostatic interaction of two particles in the suspension (of two micelles in the solution). The empirical factor 3 before u_{el} accounts for the presence of several nearest neighbors of a given particle. (In Ref. [23] this factor is missing because of a misprint, but it has been used in the computations reported therein.) It has been proven that the interaction energy $u_{el}(r)$ can be calculated from the expression [23]:

$$\frac{u_{el}(r)}{kT} = \frac{r}{4L_B}\left[\frac{e}{kT}\psi(r/2)\right]^2 \tag{4}$$

where $\psi(r)$ is the distribution of the electrostatic potential around a *single* particle in the suspension; $L_B \equiv e^2/(4\pi\varepsilon_0\varepsilon kT)$ is the Bjerrum length

($L_B = 0.72$ nm for water at 25 °C); ε_0 is the permittivity of vacuum; ε is the dielectric constant of the solvent (water); e is the elementary charge. Eq. (4) reduces the two-particle problem to the single-particle problem.

Coincidence between d_{eff} calculated from Eqs. (3), (4) and Δh measured for stratifying films has been established [23], if $\psi(r)$ is calculated by using the *jellium approximation*. In the framework of this approximation, which has been introduced in the theory of charged particle suspensions by Beresford-Smith et al. [85,86], the electric field around a given particle is calculated by assuming Boltzmann distribution of the small ions around the macroion, but *uniform* distribution of the macroions (particles). In other words, only the small ions take part in the Debye screening of the electric field of a given particle in the suspension. The jellium approximation leads to the following expression for the Debye screening parameter, κ:

$$\kappa^2 = \frac{2e^2}{\varepsilon_0 \varepsilon kT}\left(I + \frac{1}{2}Zc_p\right) \tag{5}$$

where Z is the charge of the macroions (in e units) and I is the ionic strength due to the background electrolyte. For micellar solutions, $I = \text{CMC} + \text{concentration of added salt (if any)}$. Eq. (5) is widely used in the theory of charged particle suspensions and micellar solutions [17,87,88].

In Ref. [23], it was established that in the concentration range where stratifying films are observed, $d_{eff} = c_p^{-1/3} = \Delta h$, where d_{eff} is calculated from Eqs. (3) and (4) and Δh is experimentally determined from the stratification steps, like those in Fig. 2. In contrast, for $d_{eff} < c_p^{-1/3}$ the foam films do not stratify and the oscillations of disjoining pressure vanish.

3.3. Results for N_{agg} and discussion

Table 3 shows the values of N_{agg}, calculated from the data for Δh in Table 2 using Eq. (2). The third column of Table 3 indicates that the obtained values of N_{agg} compare well with results obtained by other authors using other methods. At the best of our knowledge, here N_{agg} is determined for the first time for KMy.

Despite the large value, $N_{agg} = 135$ at 50 mM CTAB, the respective micelles are still spherical (rather than elongated). This has been established by direct observations by cryo-TEM [89]. This can be also confirmed by molecular-packing considerations. Indeed, the maximal radius of the micelle at the level of the headgroups is equal to the length of the extended CTAB molecule, $R_H = 2.85$ nm. The respective maximal surface area is $4\pi R_H^2 = 102.1$ nm^2. By molecular-size considerations, one can obtain 0.38 nm^2 for the cross-sectional area of a CTAB headgroup [90]. Dividing the maximal surface area to the minimal area per headgroup, we calculate that the maximal possible aggregation number for a spherical micelle is $N_{agg,max} \approx 269$. The greatest value $N_{agg} = 140$ for CTAB in Table 3 is smaller than 269, and consequently the respective micelles can be spherical. (In the opposite case, the micelles should be non-spherical.)

The spherical shape of the CTAB micelles is supported by the additional fact that at $c_s = 50$ mM (and at all other studied concentrations), the heights of the steps are equal: $\Delta h_1 = \Delta h_2 = \Delta h_3 = \Delta h_4$, where $\Delta h_n \equiv h_n - h_{n-1}$, $n = 1, \ldots, 4$. If the micelles were elongated, then Δh_n would be smaller for the smaller n, as indicated by the experiment [24].

The values of N_{agg} for SLES-1EO, SLES-3EO and KMy in Table 3 seem reasonable. Indeed, the surfactant with the largest headgroup, SLES-3EO, has the smallest N_{agg}, whereas the surfactant with the smallest headgroup, KMy, has the greatest N_{agg}. In addition, SLES-1EO has a slightly greater N_{agg} than SDS (Table 3). This could be explained with the fact that SLES-1EO has almost the same headgroup cross-sectional area as SDS, but its molecule is longer and the respective micelle surface area is greater, so that it can accommodate more headgroups than SDS. The bigger headgroup of SLES-3EO leads to smaller N_{agg} as compared to SLES-1EO.

Table 3
N_{agg}, α and Z determined from the values of Δh and h_0 in Table 2.

c_s (mM)	Aggregation number		Ionization degree		Charge[a]
	N_{agg} from Eq. (2)	N_{agg} from literature	α from Section 4	α from literature	Z (e units)
SDS					
30	48	50 [72], 55 [91], 59 [92]	0.46	–	22
40	61	60 [59], 62 [93], 64 [92]	0.55	–	33
50	65	64 [38,72,92], 65 [94]	0.53	0.50 [54], 0.54 [41,42]	35
100	65	65 [58], 70 [72], 73 [94]	0.56	–	37
CTAB					
10	95	88 [58], 92 [95], 95 [64,96], 98 [97]	0.20	0.19 [98], 0.22 [30,99,100]	19
20	119	–	0.23	0.23 [51], 0.24 [21,99]	27
30	137	100 [96]	0.26	0.25 [55,101]	35
40	136	–	0.26	0.28 [34]	35
50	135	139 [102], 140 [96]	0.29	0.29 [97,103], 0.32 [36], 0.34 [35]	40
CPC					
10	52	45-90 [104], 56 [40]	0.30	–	15
20	75	78 [23]	0.32	–	24
30	80	82 [97]	0.35	–	28
40	93	–	0.36	–	33
50	93	87 [71]	0.37	0.37 [97], 0.44 [40]	34
SLES-1EO					
40	67	–	0.44	–	29
50	71	–	0.48	–	34
60	79	–	0.54	–	42
SLES-3EO					
30	46	42 [62]	0.71	0.70 [61]	33
40	47	–	0.61	–	29
50	54	–	0.62	–	33
100	61	–	0.70	–	42
KMy					
50	82	–	0.33	–	27
100	84	–	0.46	–	39

[a] The values of $Z = \alpha N_{agg}$ correspond to N_{agg} from Eq. (2) and α from Section 4.

The proposed method for determining N_{agg} is applicable to all surfactant concentrations at which the foam films stratify and the ionic micelles are spherical. For non-spherical micelles, the conditions $\Delta h_n = \Delta h = \text{const.}$ and $\Delta h = c_p^{-1/3}$ could be violated [24].

4. Determination of α and Z from the experimental value of h_0

4.1. Basic equations

The following procedure for determination of α and Z was used. (i) The experimental value of the final film thickness, $h_{0,exp}$ is measured by the SE cell (Section 2). (ii) The theoretical dependence of the final film thickness on the degree of micelle ionization, $h_0(\alpha)$, is calculated (see below). (iii) From the equation $h_0(\alpha) = h_{0,exp}$, the degree of micelle ionization, α, is determined. (iv) Finally, the micelle charge is $Z = \alpha N_{agg}$.

Physically, h_0 depends on α because the counterions dissociated from the micelles in the bulk increase the Debye screening of the electrostatic repulsion and increase the osmotic pressure of the bulk phase, which leads to a decrease of the film thickness h_0 with the rise of micelle ionization, α.

The key step in the above procedure is to accurately calculate the theoretical dependence $h_0(\alpha)$. This dependence is obtained from the

equation:

$$\Pi(h_0, \alpha) = P_c. \tag{6}$$

Here, Π is the disjoining pressure of the foam film in its final state, which depends on the film thickness, h_0, and on the degree of micelle ionization, α. Eq. (6) expresses a condition for mechanical equilibrium of the liquid film stating that the disjoining pressure must be equal to the capillary pressure of the adjacent meniscus P_c [105]. For the investigated systems, the values of P_c are given in Table 1. At known dependence $\Pi(h_0, \alpha)$ and given P_c, Eq. (6) allows one to calculate h_0 at each given value of α. The respective dependence $h_0(\alpha)$ is obtained by numerical solution of Eq. (6).

In accordance with the theory by Derjaguin, Landau, Verwey and Overbeek (DLVO) [106,107], Π can be expressed as a sum of components originating from the van der Waals and electrostatic (double layer) surface forces:

$$\Pi(h, \alpha) = \Pi_{vw}(h) + \Pi_{el}(h, \alpha). \tag{7}$$

The depletion interaction due to the micelles in the Plateau border is taken into account in Π_{el} (see below). The van der Waals component can be accurately calculated from the equation

$$\Pi_{vw}(h) = -\frac{A(h)}{6\pi h^3}. \tag{8}$$

The Hamaker parameter $A(h)$ depends on the film thickness, h, because of the electromagnetic retardation effect, as follows [108]:

$$A = 2\kappa h A_0 \exp(-2\kappa h) + \frac{3h_P \nu_e}{4\pi} \frac{\left(n_w^2 - 1\right)^2}{\left(n_w^2 + 1\right)^{3/2}} \int_0^\infty \frac{\left(1 + 2\hat{h}z\right)}{\left(1 + 2z^2\right)^2} \exp\left(-2\hat{h}z\right) dz. \tag{9}$$

Here, $h_P = 6.63 \times 10^{-34}$ J·s is the Plank constant; $\nu_e = 3 \times 10^{15}$ Hz is the main electronic absorption frequency; $n_w \approx 1.333$ is the refractive index of water; $c_0 = 3.0 \times 10^8$ m/s is the speed of light in vacuum; $\hat{h} \equiv 2\pi\nu_e h n_w \left(n_w^2 + 1\right)^{1/2} / c_0$ is a dimensionless thickness; z is an integration variable; and A_0 is the "zero-frequency" contribution to $A(h)$. In our case, the contribution of the term with A_0 is negligible because the orientation and induction interactions are screened by the electrolyte [9], which is taken into account by the factor $\exp(-2\kappa h)$ in Eq. (9).

The electrostatic component of disjoining pressure equals the difference between the osmotic pressures in the midplane of the film and in the bulk solution [106–109]:

$$\Pi_{el} = (P_{osm})_{midplane} - (P_{osm})_{bulk}. \tag{10}$$

The bulk osmotic pressure can be estimated from the expression:

$$(P_{osm})_{bulk} = kT\left[2(c_1 + c_3) + (Z + 1)c_p\right]. \tag{11}$$

As usual, $Z = \alpha N_{agg}$, where N_{agg} is given in Table 3; the first term in the brackets in Eq. (11) expresses the contribution of the background electrolyte: c_1 is the concentration of surfactant monomers, c_3 is the concentration of added electrolyte, and the multiplier 2 accounts for their counterions. The second term in the brackets is the contribution of the micelles (c_p) and of the counterions dissociated from them (Zc_p).

As already mentioned, the film thickness h_0 is large enough for the micelles to enter the film, i.e. $h_0 - h_a > h_a$, see Tables 1 and 2, and Fig. 5. However, the concentration of micelles in the film is very low, because they experience a strong electrostatic repulsion from the like-charged film surfaces. In Ref. [23], we carried out calculations using two versions of the model: with and without micelles in the final film. The results showed that the model corresponding to Fig. 5 gives a better agreement with the experiment. For this reason, here we are using the latter model, which leads to the following expression for the osmotic pressure in the film's midplane:

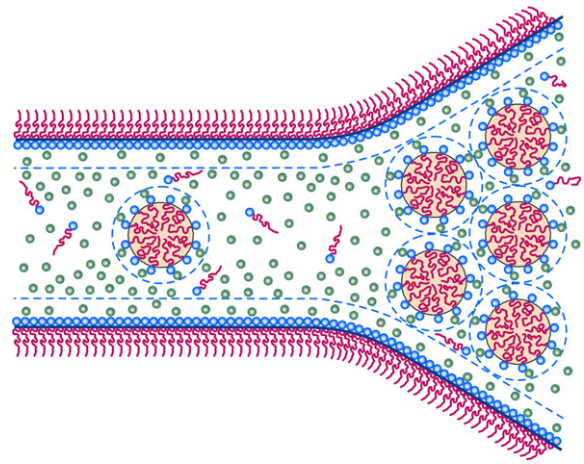

Fig. 5. The final state of the film with thickness h_0, which is affected by the concentration of counterions dissociated from the micelles in the Plateau border. Isolated micelles can be present in the film, but their concentration is rather low because they experience a strong electrostatic repulsion from the film surfaces.

$$(P_{osm})_{midplane} = kT\left[(c_1 + c_3)\left(e^{\Phi_m} + e^{-\Phi_m}\right) + Zc_p e^{\Phi_m} + c_p e^{-Z\Phi_m}\right]. \tag{12}$$

$\Phi_m = e|\psi_m|/(kT)$ is the dimensionless electrostatic potential in the midplane of the film; ψ_m is the respective dimensional potential. The Poisson–Boltzmann equation for the film (Fig. 5) can be presented in the form:

$$\frac{d^2\Phi}{dx^2} = 4\pi L_B\left[2(c_1 + c_3)\sinh\Phi + Zc_p\left(e^{\Phi} - e^{-Z\Phi}\right)\right]. \tag{13}$$

Here, $\Phi = e|\psi|/(kT)$ is the dimensionless electrostatic potential; the x-axis is perpendicular to the film surfaces and $x = 0$ corresponds to the midplane. To take a first integral, we multiply Eq. (13) by $2d\Phi/dx$ and integrate from $x = 0$ to an arbitrary x:

$$\left(\frac{d\Phi}{dx}\right)^2 = 8\pi L_B F(\Phi, \Phi_m) \tag{14}$$

$$F(\Phi, \Phi_m) \equiv 2(c_1 + c_3)(\cosh\Phi - \cosh\Phi_m) + Zc_p\left(e^{\Phi} - e^{\Phi_m}\right) + c_p\left(e^{-Z\Phi} - e^{-Z\Phi_m}\right). \tag{15}$$

In Eq. (14), the boundary condition $(d\Phi/dx)_{x=0} = 0$ has been used. Furthermore, we take square root of Eq. (14) and integrate from the midplane $x = 0$ to the film surface at $x = \tilde{h}/2$:

$$(2\pi L_B)^{1/2}\tilde{h} = \int_{\Phi_m}^{\Phi_s} [F(\Phi, \Phi_m)]^{-1/2} d\Phi \tag{16}$$

where $\tilde{h} = h - h_a$ is the thickness of the aqueous core of the film; h is the full film thickness, including the two surfactant adsorption layers, each of them of thickness $h_a/2$, see Table 1; Φ_s is the dimensionless electrostatic potential at the film surface.

4.2. Determination of Φ_s

The electric potential at the film surfaces, Φ_s, can be determined in two ways. First, Φ_s can be determined from the equation [23]:

$$\frac{\Gamma_1}{1+K_{St}\gamma_{\pm}c_2\exp\Phi_s}=\left[\frac{1}{2\pi L_B}F(\Phi_s,\Phi_m)\right]^{1/2}. \quad (17)$$

c_2 is the counterion concentration. The left-hand side of Eq. (17) represents the film surface charge density expressed through the Stern equation of counterion binding, whereas the right-hand side of Eq. (17) represents the same quantity expressed through the Gouy equation for the film, which relates the surface charge with the surface potential; $\gamma_{\pm}$ is the activity coefficient; for details see [23]. The adsorption at CMC, Γ_1, and the Stern constant, K_{St}, have been determined from fits of surface-tension isotherms. The values of K_{St} are 0.653, 7.45 and 5.93 M^{-1}, respectively, for SDS, CTAB and CPC; see Refs. [23,90,110–112]. Note that the effect of counterion binding to the surfactant headgroups at the film surface is taken into account by the term with K_{St} in Eq. (17). Solving numerically Eq. (6), along with Eqs. (7)–(12) and (15)–(17), we can determine the dependence $h_0(\alpha)$.

In Ref. [23], the dependence $\alpha(c_s)$ was calculated by solving the problem about the distribution of the electric potential around a micelle in the bulk of solution in the framework of the jellium approximation. The calculated $h_0(\alpha(c_s))$ dependence is in excellent agreement with the experimental h_0-vs. -c_s data without using any adjustable parameters. The latter fact confirms the correctness of the used theoretical model.

The calculations for SDS, CTAB and CPC [23] indicated that the theoretical dependence $h_0(\alpha)$ is not so sensitive to the value of the *film* surface potential, Φ_s. The above theoretical model predicts not only $h_0(\alpha)$, but also $\Phi_s(\alpha)$. Typical calculated curves $\Phi_s(\alpha)$ are shown in Fig. 7. One sees that Φ_s is not too sensitive to the variation of α. All these facts allow us to considerably simplify the procedure. Indeed, instead of using Eq. (17), we can substitute a constant value:

$$\Phi_s = 5.5 \quad (18)$$

This is an average value for all investigated ionic surfactants that corresponds to $|\psi_s|=141.4$ mV, which is a typical value for the surface potential of ionic surfactant solutions. (At 25 °C, the scaling factor is $kT/e\approx25.7$ mV.) For comparison, the maximal surface potential of SDS adsorption layers at an air/water interface is $|\psi_s|\approx180$ mV at 2 mM SDS, but at higher SDS concentrations, $|\psi_s|$ decreases because of the increased concentration of binding Na^+ counterions; see e.g. Fig. 6a in Ref. [111].

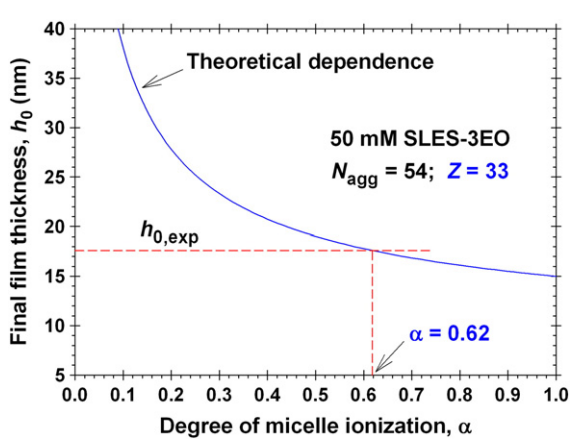

Fig. 6. Plot of the final film thickness, h_0, vs. the degree of micelle ionization, α. The solid line represents the theoretical dependence $h_0(\alpha)$ calculated as explained in the text. Using the experimental value $h_{0,exp}$ from Table 2, we determine the respective value of α as shown in the figure. The illustrative example is for 50 mM SLES-3EO, for which the values $\alpha=0.62$ and $Z=\alpha N_{agg}=33$ are obtained.

The procedure of calculations is as follows. At a given α and concentrations c_1, c_3 and c_p, we calculate $\Pi_{el}(\Phi_m)$ from Eqs. (10)–(12). Next, from Eqs. (15) and (16) we calculate the dependence $h(\Phi_m)$, where Φ_s is determined from either Eq. (17) or (18). Thus, we obtain the dependence $\Pi_{el}(h)$ in a parametric form: $\Pi_{el}=\Pi_{el}(\Phi_m)$ and $h=h(\Phi_m)$. Furthermore, $\Pi=\Pi_{el}+\Pi_{wv}$ is calculated using Eqs. (8) and (9). By variation of Φ_m, we find the value of this parameter for which $\Pi=P_c$, i.e. Eq. (6) is satisfied. The respective value of $h=h_0$ is plotted as a function of α; see Fig. 6. Finally, from the experimental thickness of the final film, $h_{0,exp}$, we determine the respective value of α as illustrated in Fig. 6.

Results for α and Z calculated using alternatively Eq. (17) or (18) are shown in Table 4. One sees that the two approaches give very close results, the greatest differences being at the highest concentrations. The use of Eq. (18) leads to a considerable simplification of the procedure for determining α and Z not only because Eq. (18) is much simpler than Eq. (17), but also because it is not necessary to determine K_{St} and Γ_1 in Eq. (17) from fits of additional data for the surface tension of the respective surfactant solutions. Thus, Eq. (18) enables one to determine α and Z only from the data for stratifying films (see Fig. 2).

As an additional verification of the correctness of the theoretical model and of the obtained values of α, we compared the theoretical disjoining pressure isotherm $\Pi(h)$ with the experimental $\Pi(h)$ isotherm independently measured by means of the Mysels–Jones porous-plate cell [113], known also as thin film pressure balance (TFPB). Additional information on this method can be found in Refs. [21,114]. The theoretical $\Pi(h)$ dependencies (the solid lines in Fig. 8) are calculated from Eqs. (7)–(12) and (15)–(17) with the values of Z from the fourth column of Table 4 calculated using Eq. (17) (the Stern counterion binding model). Fig. 8 illustrates the agreement between theory and experiment for the investigated SDS solutions at concentrations 30, 40, 50 and 100 mM. The horizontal error bars reflect the scattering of the experimental data for the film thickness h, which are most probably due to small variations in the applied sucking pressure. The scattering is the smallest for the thinnest film at 100 mM SDS. In all cases, the theoretical curves comply very well with the experimental data (Fig. 8); no adjustable parameters have been used. This agreement confirms not only the adequacy of the theoretical model, but also the correctness of the N_{agg} values determined from Eq. (2); see Table 3. (We recall that the used charge values are calculated from the expression $Z=\alpha N_{agg}$.)

Table 4
α and Z vs. the surfactant concentration c_s — comparison of the two ways of calculation.

c_s (mM)	Ionization degree, α		Charge, Z (e units)	
	From Eq. (17)	From Eq. (18)	From Eq. (17)	From Eq. (18)
SDS				
30	0.46	0.46	22	22
40	0.54	0.55	33	33
50	0.52	0.53	34	35
100	0.54	0.56	35	37
CTAB				
10	0.20	0.20	19	19
20	0.23	0.23	27	27
30	0.25	0.26	34	35
40	0.25	0.26	34	35
50	0.27	0.29	37	40
CPC				
10	0.29	0.30	15	15
20	0.31	0.32	24	24
30	0.33	0.35	26	28
40	0.33	0.36	31	33
50	0.34	0.37	31	34

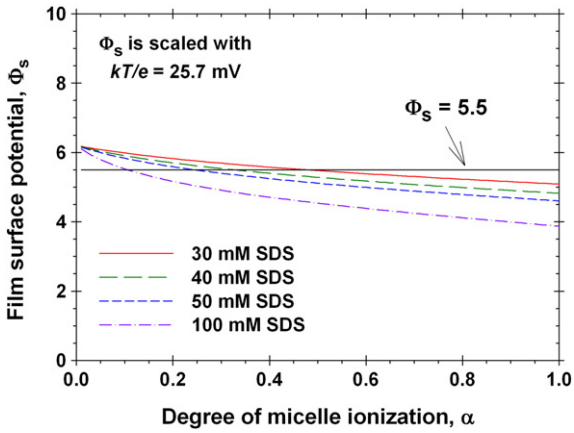

Fig. 7. Theoretical dependencies of the dimensionless surface potential of the film, $\Phi_s = e|\psi_s|/(kT)$, on the micelle ionization degree, α, calculated using the system of Eqs. (6)–(12) and (15)–(17), and the values of N_{agg} determined from Eq. (2); see Table 3. The calculations are carried out for the thinnest equilibrium films that are in contact with the respective micellar solution, but do not contain micellar layers.

5. Results and discussion

5.1. Degree of ionization, charge and aggregation number

Fig. 6 illustrates the determination of α from the theoretical curve $h_0(\alpha)$ and from the experimental value of the final film thickness $h_{0,exp}$ taken from Table 2. In this figure, the determination of α is illustrated for 50 mM surfactant concentration; the results for all surfactant concentrations, obtained in a similar way, are given in Table 3.

In Fig. 6, h_0 decreases with the rise of α. As mentioned above, this is related to the fact that a greater degree of ionization of the micelles in the bulk leads to a higher sucking osmotic pressure due to the counterions dissociated from the micelles; see Eq. (11). The slope of the $h_0(\alpha)$ dependence decreases with the rise of α (Fig. 6). For this reason, the accuracy of determination of α from $h_{0,exp}$ decreases with the increase of α.

Figs. 9 and 10 compare the obtained results for N_{agg}, α and $Z = \alpha N_{agg}$ for the investigated surfactants: SDS, CTAB, CPC, SLES-1EO, SLES-3EO and KMy. The general trend is that all these quantities are to increase with the rise of the surfactant concentration, c_s, and to level off at higher concentrations. It is remarkable that the surfactants

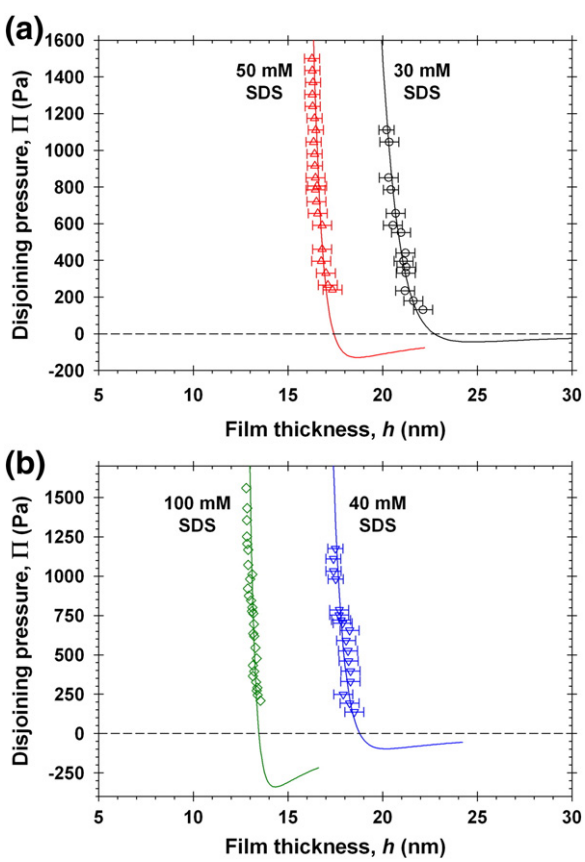

Fig. 8. Comparison of theoretically calculated dependencies of the disjoining pressure Π vs. the film thickness h (the solid lines) with experimental data for $\Pi(h)$ obtained by the Mysels–Jones porous plate method. The data refer to the leftmost branch of the $\Pi(h)$ dependence, that with $h = h_0$, which corresponds to a film that does not contain micellar layers. The used solutions are (a) 30 and 50 mM SDS and (b) 40 and 100 mM SDS.

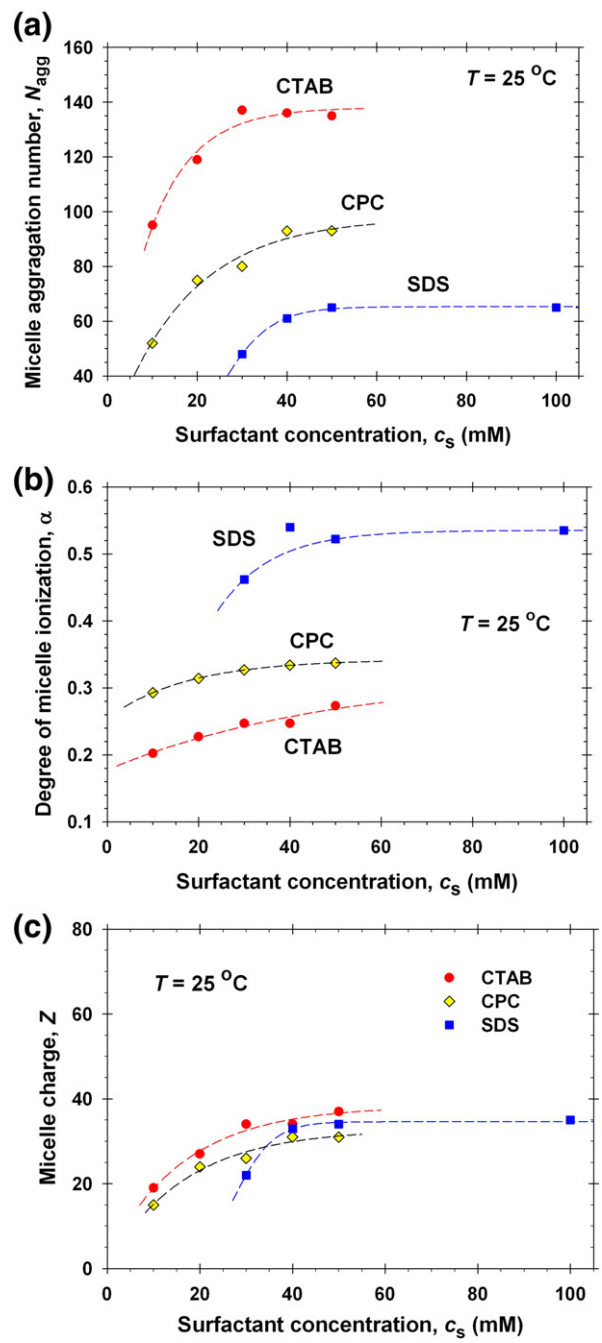

Fig. 9. Comparison of the obtained results for SDS, CTAB and CPC. (a) Plots of N_{agg} vs. c_s. (b) Plots of α vs. c_s. (c) Plots of Z vs. c_s. The data are from Table 3, and the lines are guides to the eye.

with greater N_{agg} have smaller α, so that the values of $Z = \alpha N_{agg}$ are not so different (Figs. 9 and 10). This experimental fact is discussed in Section 5.2.

The obtained values of α compare very well with data obtained by other authors using other methods; see Table 3. For example, for SDS we obtain micelle ionization in the range $\alpha = 0.46$–0.54; similar values have been reported in the literature: $\alpha = 0.50$ obtained by ζ-potential measurements [54] and $\alpha = 0.54$ from the mass action law [42].

Likewise, for CTAB we obtain micelle ionization in the range $\alpha = 0.20$–0.27; similar values have been reported in the literature: $\alpha = 0.23$ obtained from the Krafft temperature [51] and $\alpha = 0.25$ determined by chemical trapping of free counterions by a water soluble arenediazonium salt [55].

The results for N_{agg}, α and Z obtained here for SLES-1EO, SLES-3EO and KMy are novel and they will be verified in future experiments by other methods (Fig. 10).

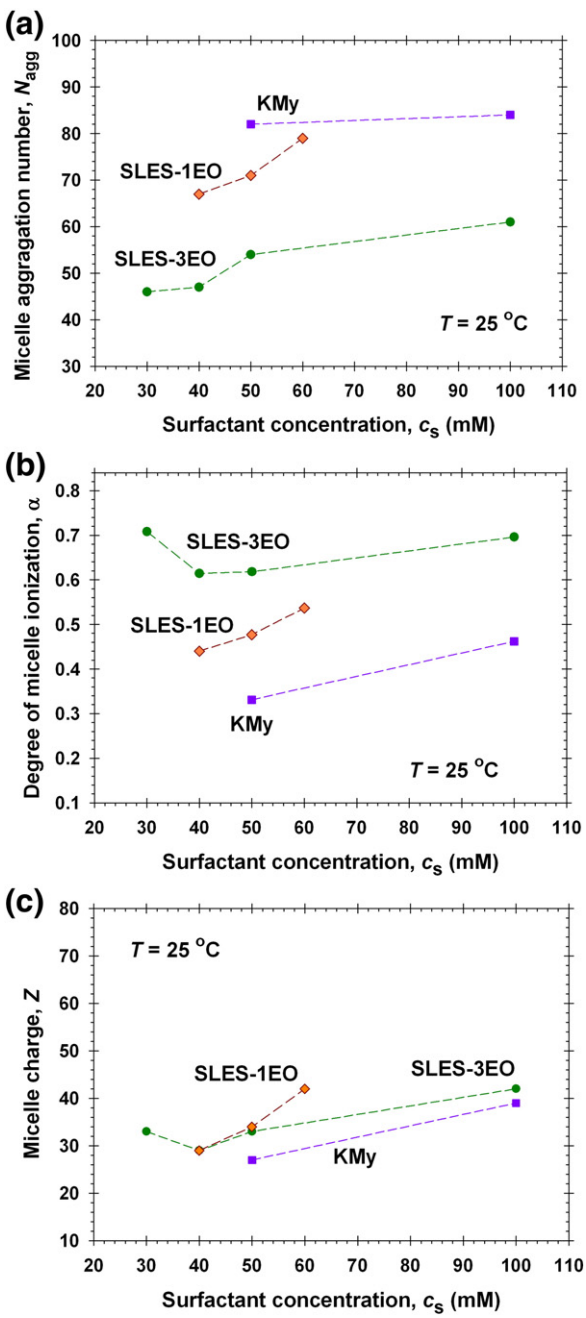

Fig. 10. Comparison of the obtained results for SLES-1EO, SLES-3EO and KMy. (a) Plots of N_{agg} vs. c_s. (b) Plots of α vs. c_s. (c) Plots of Z vs. c_s. The data are from Table 3, and the lines are guides to the eye.

5.2. Why larger N_{agg} corresponds to smaller α?

The surface charge of a micelle is determined by the balance of two opposite tendencies. Here, this is illustrated for the analogous case of flat interface, for which the equations are simpler.

The first tendency is the surface potential to grow with the surface charge, which is described by the Gouy equation [115]. For a flat surfactant adsorption layer, this equation can be presented in the form [116]:

$$\alpha(\Phi_s) = \frac{4}{\kappa_c \Gamma}\sqrt{I}\sinh\left(\frac{\Phi_s}{2}\right) \text{(Gouy equation)}. \tag{19}$$

As before, Φ_s is the surface potential; I is the ionic strength of a 1:1 electrolyte; $\kappa_c = (8\pi L_B)^{1/2}$ is a constant parameter, which is equal to 1.345×10^{-4} m$^{1/2}$ for water solutions at 25 °C; Γ is adsorption (number of surfactant molecules per unit area); for micelles, $\Gamma = N_{agg}/(4\pi R^2)$, where R is the micelle radius. Eq. (19) is known also as the Graham equation [117].

The second tendency is related to the effect of counterion binding, which is described by the Stern equation [118] and leads to the following expression for the degree of ionization [23]:

$$\alpha(\Phi_s) = \frac{1}{1 + K_{St} I \exp(\Phi_s)} \text{(Stern equation)}. \tag{20}$$

K_{St} is the Stern constant. Eq. (20) represents α as a decreasing function of Φ_s. Physically, at higher Φ_s more counterions are attracted by the surface, where they bind and decrease the ionization α. The curves in Fig. 11 are drawn with typical parameter values: $K_{St} = 0.6476$ M^{-1} for SDS [116]; $I = 8$ mM; $\Gamma_1 = 1$ μmol/m^2 and $\Gamma_2 = 4$ μmol/m^2.

The balance of the aforementioned two tendencies corresponds to the intersection point of the $\alpha(\Phi_s)$ curves calculated from Eqs. (19) and (20); see Fig. 11. These curves refer to the same ionic strength I (which could be controlled by the addition of salt), but to two different values of Γ (which could be due to different sizes of the surfactant headgroups). Note that Γ enters only Eq. (19), which predicts a lower $\alpha(\Phi_s)$ for the greater value of Γ. As seen in Fig. 11, $\Gamma_2 > \Gamma_1$ corresponds to $\alpha_2 < \alpha_1$, i.e. the degree of ionization is smaller for the surface of greater surfactant adsorption. (For micelles of the same R, greater Γ

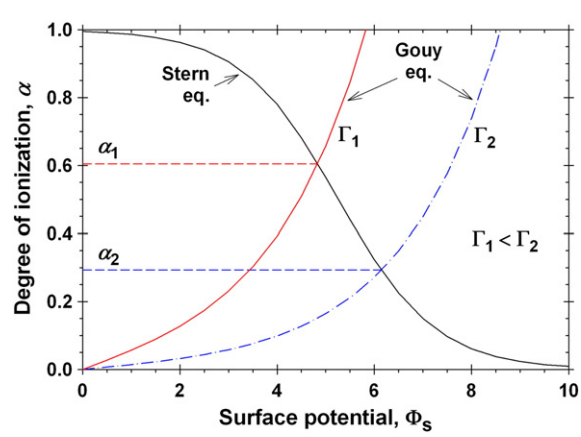

Fig. 11. Plots of α vs. the dimensionless surface potential, Φ_s, calculated from the Gouy and Stern equations, Eqs. (19) and (20) for two surface densities of surfactant molecules, $\Gamma_1 < \Gamma_2$. The intersection points determine the respective values of the ionization degree, α_1 and α_2.

corresponds to greater N_{agg}.) The data in Figs. 9 and 10 show that the same tendency is observed also for micelles, i.e. larger N_{agg} corresponds to smaller α.

In the case of micelles, the full system of equations should include the generalization of Eq. (19) for a spherical interface [119], and should also take into account the contribution of the dissociated counterions into the ionic strength I, which leads to an additional link between I and α.

6. Conclusions

A new method is developed, which allows one to determine the aggregation number, N_{agg}, and charge, Z, of ionic surfactant micelles from the height of the step, Δh, and the final thickness, h_0, of stratifying foam films. The method is applied to determine N_{agg} and Z for micelles of SDS, CTAB, CPC (data from Ref. [23]), as well as of SLES-1EO, SLES-3EO, and KMy (new data) at various surfactant concentrations, c_s, and the results are analyzed.

The determination of N_{agg} and Z (and $\alpha = Z/N_{agg}$) from film-stratification data, which is proposed in the present article, has the following advantages:

(i) N_{agg} and Z are determined simultaneously, from the same set of experimental data;
(ii) N_{agg} and Z are obtained at each given surfactant concentration. (They are not average values for the whole micellar concentration range, as the values obtained from electrolytic conductivity measurements or from the dependence of CMC on the salt concentration.);
(iii) N_{agg} and Z can be determined even for turbid solutions, like those of carboxylates, where the micelles coexist with crystallites and the light-scattering and fluorescence methods are inapplicable.

The main limitations of the method are that the foam films must stratify and the micelles have to be spherical. This is fulfilled if the surfactant concentration is sufficiently high, but not too high (to avoid formation of non-spherical micelles), and the concentration of added salt (which suppresses the stratification) should be sufficiently low. These requirements are satisfied for numerous systems that represent scientific and practical interest.

Acknowledgments

We thankfully acknowledge the support from the National Science Fund of Bulgaria, grant No. DID-02-18/2009; from Unilever R&D, Trumbull, USA; from the FP7 project Beyond-Everest, and from COST Action CM1101 of the ESF. The authors are grateful to Ms. Mariana Paraskova for her assistance in the figure preparation.

References

[1] Nikolov AD, Wasan DT, Kralchevsky PA, Ivanov IB. Ordered structures in thinning micellar foam and latex films. In: Ise N, Sogami I, editors. Ordering and organisation in ionic solutions. Singapore: World Scientific; 1988. p. 302-14.
[2] Nikolov AD, Wasan DT. Ordered micelle structuring in thin films from anionic surfactant solutions: I. Experimental. J Colloid Interface Sci 1989;133:1–12.
[3] Nikolov AD, Kralchevsky PA, Ivanov IB, Wasan DT. Ordered micelle structuring in thin films from anionic surfactant solutions: II. Model development. J Colloid Interface Sci 1989;133:13-22.
[4] Kralchevsky PA, Nikolov AD, Wasan DT, Ivanov IB. Formation and expansion of dark spots in stratifying foam films. Langmuir 1990;6:1180-9.
[5] Denkov ND, Yoshimura H, Nagayama K, Kouyama T. Nanoparticle arrays in freely suspended vitrified films. Phys Rev Lett 1996;76:2354-7.
[6] Horn RG, Israelachvili JN. Direct measurement of structural forces between two surfaces in a nonpolar liquid. J Chem Phys 1981;75:1400-11.
[7] Christenson HK, Gruen DWR, Horn RG, Israelachvili JN. Structuring in liquid alkanes between solid surfaces: force measurements and mean-field theory. J Chem Phys 1987;87:1834-41.
[8] Israelachvili JN, Pashley RM. Molecular layering of water at surfaces and origin of repulsive hydration forces. Nature 1983;306:249-50.
[9] Israelachvili JN. Intermolecular and surface forces. London: Academic Press; 1992.
[10] Kralchevsky PA, Denkov ND. Analytical expression for the oscillatory structural surface force. Chem Phys Lett 1995;240:385-92.
[11] Henderson D. An explicit expression for the solvent contribution to the force between colloidal particles using a hard sphere model. J Colloid Interface Sci 1988;121:486-90.
[12] Kjellander R, Sarman S. On the statistical mechanics of inhomogeneous fluids in narrow slits. An application to a hard-sphere fluid between hard walls. Chem Phys Lett 1988;149:102-8.
[13] Pollard ML, Radke CJ. Density-functional modeling of structure and forces in thin micellar liquid films. J Chem Phys 1994;101:6979-91.
[14] Trokhymchuk A, Henderson D, Nikolov A, Wasan DT. A simple calculation of structural and depletion forces for fluids/suspensions confined in a film. Langmuir 2001;17:4940-7.
[15] Chu XL, Nikolov AD, Wasan DT. Monte Carlo simulation of inlayer structure formation in thin liquid films. Langmuir 1994;10:4403-8.
[16] Klapp SHL, Zeng Y, Qu D, von Klitzing R. Surviving structure in colloidal suspensions squeezed from 3D to 2D. Phys Rev Lett 2008;100:118303.
[17] Klapp SHL, Qu D, von Klitzing R. Long-range interactions between soft colloidal particles in slit – pore geometries. J Phys Chem B 2007;111:1296-303.
[18] Klapp SHL, Grandner S, Zeng Y, von Klitzing R. Asymptotic structure of charged colloids between two and three dimensions: the influence of salt. J Phys Condens Matter 2008;20:494232.
[19] Grandner S, Zeng Y, von Klitzing R, Klapp SHL. Impact of surface charges on the solvation forces in confined colloidal solutions. J Chem Phys 2009;131:154702.
[20] Grandner S, Klapp SHL. Surface-charge-induced freezing of colloidal suspensions. EPL-Europhys Lett 2010;90:68004.
[21] Basheva ES, Kralchevsky PA, Danov KD, Ananthapadmanabhan KP, Lips A. The colloid structural forces as a tool for particle characterization and control of dispersion stability. Phys Chem Chem Phys 2007;9:5183-98.
[22] Wasan D, Nikolov A. Thin liquid films containing micelles or nanoparticles. Curr Opin Colloid Interface Sci 2008;13:128-33.
[23] Danov KD, Basheva ES, Kralchevsky PA, Ananthapadmanabhan KP, Lips A. The metastable states of foam films containing electrically charged micelles or particles: experiment and quantitative interpretation. Adv Colloid Interface Sci 2011;168:50-70.
[24] Christov NC, Danov KD, Zeng Y, Kralchevsky PA, von Klitzing R. Oscillatory structural forces due to nonionic surfactant micelles: data by colloidal-probe AFM vs. theory. Langmuir 2010;26:915-23.
[25] Trokhymchuk A, Henderson D, Nikolov AD, Wasan DT. Computer modeling of ionic micelle structuring in thin films. J Phys Chem B 2003;107:3927-37.
[26] Trokhymchuk A, Henderson D, Nikolov A, Wasan DT. Computer simulation of macroion layering in a wedge film. Langmuir 2005;21:10240-50.
[27] Piech M, Walz JY. The structuring of nonadsorbed nanoparticles and polyelectrolyte chains in the gap between a colloidal particle and plate. J Phys Chem B 2004;108:9177-88.
[28] Tulpar A, Van Tassel PR, Walz JY. Structuring of macroions confined between like-charged surfaces. Langmuir 2006;22:2876-83.
[29] Zeng Y, Grandner S, Oliveira CLP, Thünemann AF, Paris O, Pedersen JS, et al. Effect of particle size and Debye length on order parameters of colloidal silica suspensions under confinement. Soft Matter 2011;7:10899-909.
[30] El Kadi N, Martins F, Clausse D, Schulz PC. Critical micelle concentrations of aqueous hexadecytrimethylammonium bromide–sodium oleate mixtures. Colloid Polym Sci 2003;281:353-62.
[31] Szymczyk K, Zdziennicka A, Janczuk B, Wojcik W. The properties of mixtures of two cationic surfactants in water at water/air interface. Colloids Surf A 2005;264:147-56.
[32] Chakraborty T, Ghosh S, Moulik SP. Micellization and related behavior of binary and ternary surfactant mixtures in aqueous medium: cetylpyridinium chloride (CPC), cetyltrimethylammonium bromide (CTAB), and polyoxyethylene (10) cetyl ether (Brij-56) derived system. J Chem Phys B 2005;109:14813-23.
[33] Azum N, Naqvi AZ, Akram M, Kabir-ud-Din. Studies of mixed micelle formation between cationic gemini and cationic conventional surfactants. J Colloid Interface Sci 2008;328:429-35.
[34] Samakande A, Chaghi R, Derrien G, Charnay C, Hartmann PC. Aqueous behaviour of cationic surfactants containing a cleavable group. J Colloid Interface Sci 2008;320:315-20.
[35] Verma SK, Ghosh KK. Micellar and surface properties of some monomeric surfactants and a gemini cationic surfactant. J Surfactants Deterg 2011;14:347-52.
[36] Akbas H, Elemenli A, Boz M. Aggregation and thermodynamic properties of some cationic gemini surfactants. J Surfactants Deterg 2012;15:33-40.
[37] Shanks PC, Franses EI. Estimation of micellization parameters of aqueous sodium dodecyl sulfate from conductivity data. J Phys Chem 1992;96:1794-805.
[38] Shah SS, Saeed A, Sharif QM. A study of micellization parameters and electrostatic interactions in micellar solution of sodium dodecyl sulfate. Colloids Surf A 1999;155:405-12.
[39] Shah SS, Jamroz NU, Sharif QM. Micellization parameters and electrostatic interactions in micellar solution of sodium dodecyl sulfate (SDS) at different temperatures. Colloids Surf A 2001;178:199-206.
[40] Bhat MA, Dar AA, Amin A, Rashid PI, Rather GM. Temperature dependence of transport and equilibrium properties of alkylpyridinium surfactants in aqueous solutions. J Chem Thermodyn 2007;39:1500-7.
[41] Corrin ML, Harkins WD. The effect of salts on the critical concentration for the formation of micelles in colloidal electrolytes. J Am Chem Soc 1947;69:683-8.
[42] Corrin ML. The effect of salts and chain length on the critical concentration of colloidal electrolytes. J Colloid Sci 1948;3:333-8.
[43] Shedlovsky L, Jakob CW, Epstein MB. Study of pNa of aqueous solutions of sodium decyl, dodecyl, and tetradecyl sulfates by E.M.F. measurements. J Phys Chem 1963;67:2075-8.

[44] Feinstein ME, Rosano HL. The determination of the apparent binding of counterions to micelles by electromotive force measurements. J Colloid Interface Sci 1967;24:73-9.
[45] Shirahama K. The membrane potentials of sodium dodecyl sulfate solutions at 25 °C. Colloid Polym Sci 1972;250:620-1.
[46] Sasaki T, Hattori M, Sasaki J, Nukina K. Studies of aqueous sodium dodecyl sulfate solutions by activity measurements. Bull Chem Soc Jpn 1975;48:1397-403.
[47] Gerakis AM, Koupparis Michael A. Physicochemical studies of the cetyltrimethylammonium bromide micellar system using a bromide selective electrode. Talanta 1994;41:765-73.
[48] Hsiao CC, Wang T-Y, Tsao H-K. Counterion condensation and release in micellar solutions. J Chem Phys 2005;122:144702.
[49] Fishman ML, Eirich FR. Interactions of aqueous poly(N-vinylpyrrolidone) with sodium dodecyl sulfate. I. Equilibrium dialysis measurements. J Phys Chem 1971;75:3135-40.
[50] Huff H, McBain JW, Brady AP. The vapor pressures of aqueous solutions of some detergents. J Phys Chem 1951;55:311-21.
[51] Vautier-Giongo C, Bales BL. Estimate of the ionization degree of ionic micelles based on Krafft temperature measurements. J Phys Chem B 2003;107:5398-403.
[52] Stigter D, Mysels KJ. Tracer electrophoresis. II. The mobility of the micelle of sodium lauryl sulfate and its interpretation in terms of zeta potential and charge. J Phys Chem 1955;59:45-51.
[53] Mysels KJ, Dulin CI. Tracer electrophoresis III. The mobility of the Na^+ constituent in sodium lauryl sulfate solutions. J Colloid Sci 1955;10:461-73.
[54] Stigter D. On density, hydration, shape, and charge of micelles of sodium dodecyl sulfate and dodecyl ammonium chloride. J Colloid Interface Sci 1967;23:379-88.
[55] Cuccovia I, da Silva IN, Chaimovich H, Romsted LS. New method for estimating the degree of ionization and counterion selectivity of cetyltrimethylammonium halide micelles: chemical trapping of free counterions by a water soluble arenediazonium ion. Langmuir 1997;13:647-52.
[56] Bales BL. A definition of the degree of ionization of a micelle based on its aggregation number. J Phys Chem B 2001;105:6798-804.
[57] Shiloach A, Blankschtein D. Measurement and prediction of ionic/nonionic mixed micelle formation and growth. Langmuir 1998;14:7166-82.
[58] Lianos P, Zana R. Fluorescence probe studies of the effect of concentration on the state of aggregation of surfactants in aqueous solution. J Colloid Interface Sci 1981;84:100-7.
[59] Gehlen MH, De Schryver FC. Fluorescence quenching in micelles in the presence of a probe-quencher ground-state charge-transfer complex. J Phys Chem 1993;97:11242-8.
[60] Bhattacharya SC, Das HT, Moulik SP. Quenching of fluorescence of 2-anthracenesulphonate by cetylpyridinium chloride in micellar solutions of Tweens, TritonX-100, sodium dodecylsulphate (SDS) and cetyltrimethylammoniumbromide (CTAB). J Photochem Photobiol A Chem 1993;71:257-62.
[61] Aoudia M, Al-Maamari T, Al-Salmi F. Intramolecular and intermolecular ion–dipole interactions in sodium lauryl ether sulfates (SLES) self-aggregation and mixed micellization with Triton X-100. Colloids Surf A 2009;335:55-61.
[62] Aoudia M, Al-Haddabi B, Al-Harthi Z, Al-Rubkhi A. Sodium lauryl ether sulfate micellization and water solubility enhancement towards naphthalene and pyrene: effect of the degree of ethoxylation. J Surfactants Deterg 2010;13:103-11.
[63] Zana R, Levy H, Danino D, Talmon Y, Kwetkat K. Mixed micellization of cetyltrimethylammonium bromide and an anionic dimeric (gemini) surfactant in aqueous solution. Langmuir 1997;13:402-8.
[64] Hansson P, Jönsson B, Ström C, Söderman O. Determination of micellar aggregation numbers in dilute surfactant systems with the fluorescence quenching method. J Phys Chem B 2000;104:3496-506.
[65] Bales BL, Ranganathan R. Characterization of mixed micelles of SDS and a sugar-based nonionic surfactant as a variable reaction medium. J Phys Chem B 2001;105:7465-73.
[66] Griffiths PC, Paul A, Heenan RK, Penfold J, Ranganathan R, Bales BL. Role of counterion concentration in determining micelle aggregation: evaluation of the combination of constraints from small-angle neutron scattering, plectron paramagnetic resonance, and time-resolved fluorescence quenching. J Phys Chem B 2004;108:3810-6.
[67] Bales BL, Messina L, Vidal A, Peric M, Nascimento OR. Precision relative aggregation number determinations of SDS micelles using a spin Probe. A model of micelle surface hydration. J Phys Chem B 1998;102:10347-58.
[68] Törnblom M, Henriksson U, Ginley M. A field dependent ^2H nuclear magnetic relaxation study of the aggregation behavior in micellar solutions of CTAB and SDS. J Phys Chem 1994;98:7041-51.
[69] Gharibi H, Sohrabi B, Javadian S, Hashemianzadeh M. Study of the electrostatic and steric contributions to the free energy of ionic/nonionic mixed micellization. Colloids Surf A 2004;244:187-96.
[70] Reiss-Husson F, Luzzati V. The structure of the micellar solutions of some amphiphilic compounds in pure water as determined by absolute small-angle X-ray scattering techniques. J Phys Chem 1964;68:3504-11.
[71] Amos DA, Lynn S, Radke CJ. A self-consistent multicomponent activity coefficient model for ionic micellar surfactant solutions. Langmuir 1998;14:2297-306.
[72] Bales BL, Almgren M. Fluorescence quenching of pyrene by Copper(II) in sodium dodecyl sulfate micelles. Effect of micelle size as controlled by surfactant concentration. J Phys Chem 1995;99:15153-62.
[73] Tzocheva SS, Kralchevsky PA, Danov KD, Georgieva GS, Post AJ, Ananthapadmanabhan KP. Solubility limits and phase diagrams for fatty acids in anionic (SLES) and zwitterionic (CAPB) micellar surfactant solutions. J Colloid Interface Sci 2012;369:274-86.
[74] Basheva ES, Stoyanov S, Denkov ND, Kasuga K, Satoh N, Tsujii K. Foam boosting by amphiphilic molecules in the presence of silicone oil. Langmuir 2001;17:969-79.
[75] Boneva MP, Danov KD, Kralchevsky PA, Kralchevska SD, Ananthapadmanabhan KP, Lips A. Coexistence of micelles and crystallites in solutions of potassium myristate: soft matter vs. solid matter. Colloids Surf A 2010;354:172-87.
[76] Scheludko A, Exerowa D. Device for interferometric measuring of the thickness of microscopic foam films. C R Acad Bulg Sci 1959;7:123-32.
[77] Sheludko A. Thin liquid films. Adv Colloid Interface Sci 1967;1:391-464.
[78] Bergeron V, Radke CJ. Equilibrium measurements of oscillatory disjoining pressures in aqueous foam films. Langmuir 1992;8:3020-6.
[79] Jönsson B, Broukhno A, Forsman J, Åkesson T. Depletion and structural forces in confined electrolyte solutions. Langmuir 2003;19:9914-22.
[80] Qu D, Pedersen JS, Garnier S, Laschewsky A, Möhwald H, von Klitzing R. Effect of polymer charge and geometrical confinement on ion distribution and the structuring in semidilute polyelectrolyte solutions: comparison between AFM and SAXS. Macromolecules 2006;39:7364-71.
[81] Qu D, Brotons G, Bosio V, Fery A, Salditt T, Langevin D, et al. Interactions across liquid thin films. Colloids Surf A 2007;303:97–109.
[82] Von Klitzing R, Thormann E, Nylander T, Langevin D, Stubenrauch C. Confinement of linear polymers, surfactants, and particles between interfaces. Adv Colloid Interface Sci 2010;155:19-31.
[83] Klapp SHL, Grandner S, Zeng Y, von Klitzing R. Charged silica suspensions as model materials for liquids in confined geometries. Soft Matter 2010;6:2330-6.
[84] Raman CV. On the mean distance between neighbouring molecules in a fluid. Philos Mag 1924;47:671-9, http://dx.doi.org/10.1080/14786442408634406.
[85] Beresford-Smith B, Chan DYC. Electrical double-layer interactions in concentrated colloidal systems. Faraday Discuss Chem Soc 1983;76:65-75.
[86] Beresford-Smith B, Chan DYC, Mitchell DJ. The electrostatic interaction in colloidal systems with low added electrolyte. J Colloid Interface Sci 1985;105:216-34.
[87] Pashley RM, Ninham BW. Double-layer forces in ionic micellar solutions. J Phys Chem 1987;91:2902-4.
[88] Richetti P, Kékicheff P. Direct measurements of depletion and structural forces of a micellar system. Phys Rev Lett 1992;68:1951-4.
[89] Singh M, Ford C, Agarwal V, Fritz G, Bose A, John VT, et al. Structural evolution in cationic micelles upon incorporation of a polar organic dopant. Langmuir 2004;20:9931-7.
[90] Valkovska DS, Shearman GC, Bain CD, Darton RC, Eastoe J. Adsorption of ionic surfactants at an expanding air–water interface. Langmuir 2004;20:4436-45.
[91] Turro NJ, Yekta A. Luminescent probes for detergent solutions. A simple procedure for determination of the mean aggregation number of micelles. J Am Chem Soc 1978;100:5951-2.
[92] Quina FH, Nassar PM, Bonilha JBS, Bales BL. Growth of sodium dodecyl sulfate micelles with detergent concentration. J Phys Chem 1995;99:17028-31.
[93] Mukerjee P, Mysels KJ. Critical micelle concentration of aqueous surfactant systems. Washington DC:Nat Stand Ref Data Ser — Nat Bur Stand (USA), 36; 1971.
[94] Benrraou M, Bales BL, Zana R. Effect of the nature of the counterion on the properties of anionic surfactants 1. J Phys Chem B 2003;107:13432-40.
[95] Weidemaier K, Tavernier HL, Fayer MD. Photoinduced electron transfer on the surfaces of micelles. J Phys Chem B 1997;101:9352-61.
[96] Van Stam J, Depaemelaere S, De Schryver FC. Micellar aggregation numbers — a fluorescence study. J Chem Educ 1998;75:93-8.
[97] Mata J, Varade D, Bahadur P. Aggregation behavior of quaternary salt based cationic surfactants. Thermochim Acta 2005;428:147-55.
[98] Larsen JW, Tepley LB. Effect of aqueous alcoholic solvents on counterion-binding to CTAB micelles. J Colloid Interface Sci 1974;49:113-8.
[99] Sepulveda L, Cortes J. Ionization degrees and critical micelle concentrations of hexadecyltrimethylammonium and tetradecyltrimethylammonium micelles with different counterions. J Phys Chem 1985;89:5322-4.
[100] Dorshow R, Briggs J, Bunton CA, Nicoli DF. Dynamic light scattering from cetyltrimethylammonium bromide micelles. Intermicellar interactions at low ionic strengths. J Phys Chem 1982;86:2388-95.
[101] Bunton CA, Romsted LS, Sepulveda L. A quantitative treatment of micellar effects upon deprotonation equilibriums. J Phys Chem 1980;84:2611-8.
[102] Hassan PA, Hodgdon TK, Sagasaki M, Fritz-Popovski G, Kaler EW. Phase behavior and microstructure evolution in aqueous mixtures of cetyltrimethylammonium bromide and sodium dodecyl tri-oxyethylene sulfate. C R Chim 2009;12:18-29.
[103] Lindman B, Puyal MC, Kamenka N, Rymden R, Stilbs P. Micelle formation of anionic and cationic surfactants from Fourier transform proton and lithium-7 nuclear magnetic resonance and tracer self-diffusion studies. J Phys Chem 1984;88:5048-57.
[104] Mukhim T, Ismail K. Micellization of cetylpyridinium chloride in aqueous lithium chloride, sodium chloride, and potassium chloride media. J Surf Sci Technol 2005;21:113-27.
[105] Toshev BV, Ivanov IB. Thermodynamics of thin liquid films. I. Basic relations and conditions for equilibrium. Colloid Polym Sci 1975;253:558-65.
[106] Derjaguin BV, Landau LD. Theory of the stability of strongly charged lyophobic sols and of the adhesion of strongly charged particles in solutions of electrolytes. Acta Physicochim URSS 1941;14:633-62.
[107] Verwey EJW, Overbeek JThG. Theory of the stability of lyophobic colloids. Amsterdam: Elsevier; 1948.
[108] Russel WB, Saville DA, Schowalter WR. Colloidal dispersions. Cambridge: Cambridge Univ. Press; 1989.

[109] Langmuir I. The role of attractive and repulsive forces in the formation of tactoids, thixotropic gels, protein crystals and coacervates. J Chem Phys 1938;6: 873-96.
[110] Kolev VL, Danov KD, Kralchevsky PA, Broze G, Mehreteab A. Comparison of the van der Waals and Frumkin adsorption isotherms for sodium dodecyl sulfate at various salt concentrations. Langmuir 2002;18:9106-9.
[111] Kralchevsky PA, Danov KD, Kolev VL, Broze G, Mehreteab A. Effect of nonionic admixtures on the adsorption of ionic surfactants at fluid interfaces. 1. Sodium dodecyl sulfate and dodecanol. Langmuir 2003;19:5004-18.
[112] Taylor CD, Valkovska DS, Bain CD. A simple and rapid method for the determination of the surface equations of state and adsorption isotherms for efficient surfactants. Phys Chem Chem Phys 2003;5:4885-91.
[113] Mysels KJ, Jones MN. Direct measurement of the variation of double-layer repulsion with distance. Discuss Faraday Soc 1966;42:42-50.
[114] Kralchevsky PA, Danov KD, Basheva ES. Hydration force due to the reduced screening of the electrostatic repulsion in few-nanometer-thick films. Curr Opin Colloid Interface Sci 2011;16:517-24.
[115] Gouy LG. Sur la constitution de la charge électrique à la surface d'un électrolyte. J Phys 1910;9:457-68. http://electrochem.cwru.edu/estir/hist/hist-21-Gouy-1.pdf.
[116] Kralchevsky PA, Danov KD, Broze G, Mehreteab A. Thermodynamics of ionic surfactant adsorption with account for the counterion binding: effect of salts of various valency. Langmuir 1999;15:2351-65.
[117] Grahame DC. Diffuse double layer theory for electrolytes of unsymmetrical valence types. J Chem Phys 1953;21:1054-60.
[118] Stern O. Zur Theorie der elektrolytischen Doppelschicht. Z Elektrochem 1924;30: 508-16 http://electrochem.cwru.edu/estir/hist/hist-81-OStern.pdf.
[119] Mitchell DJ, Ninham BW. Electrostatic curvature contributions to interfacial tension of micellar and microemulsion phases. J Phys Chem 1983;87:2996-8.